PCCP

Accepted Manuscript

ROYAL SOCIETY OF CHEMISTRY

www.rsc.org/pccp

Physical Chemistry Chemical Physics
CREATED USING THE RSC LaTeX PCCP ARTICLE TEMPLATE – SEE www.rsc.org/electronicfiles FOR DETAILS
ARTICLE TYPE www. rsc.org/xxxxxx | XXXXXXXX

A DFT study of a new class of Gold Nanocluster-Photochrome multi-functional switches†

Arnaud Fihey,* François Maurel, and Aurélie Perrier*

Received Xth XXXXXXXXXX 20XX, Accepted Xth XXXXXXXXX 20XX
First published on the web Xth XXXXXXXXXX 200X
DOI: 10.1039/b000000x

With the help of a computational scheme combining Molecular Dynamics, DFT and TD-DFT methods, the conformational, electronic and optical properties of a new class of hybrid compounds where a photochromic molecule belonging to the dithienylethene family (DTE) is covalently linked to a Au_{25} nanocluster (gold nanocluster or GNC), are investigated. We compare two types of hybrid GNC-DTE systems where the aromatic linker between the metallic and the DTE moiety is either a phenyl or a thiophene ring. By examining the perturbation of the DTE electronic structure after grafting upon the GNC, we show that the hybrid system with a phenyl linker should preserve its photochromic activity. For the latter system, we have then studied the possible energy and electron transfer between the GNC and the DTE units. The energy transfer between the two moieties can be a priori discarded while an uni-directional electron transfer should take place from the GNC to the excited DTE. We show that this transfer can be controlled by switching the state of the molecule.

1 Introduction

Among the numerous photoactive organic compounds, photochromes have aroused an increasing interest both experimentally [1–5] and theoretically [6–9] over the last decades. In these compounds, two isomers are able to undergo a light-induced reversible transformation between two isomers characterized by specific structural and electronic features. Among the different photochromic families, dithienylethene derivatives (DTEs) are one of the most effective photochromic compounds, as both isomers are generally stable at room temperature and exhibit a high switching fatigue resistance (see Figure 1(a)). Consequently, these compounds may be used as on and off states in molecular-scaled optoelectronic devices such as switches, logic gates or memories. Within these devices, DTEs are generally attached to noble metal electrodes or nanoparticles (NPs) [10–12]and should retain their photochromic characteristics after anchoring on the metallic surface in a way to provide efficient nano-switches. In the case of DTE directly attached to a 2 nm-size gold NP, Feringa and coworkers have shown that the cyclization reaction depends on the nature of the spacer linking the switching molecule to the surface of the metallic aggregate. [13] They observed that the ring-closure of the open DTE is either preserved with a phenyl linker, or inhibited with a thiophene ring one. The same observations were obtained in the case where the DTE is fixed between two gold contacts. [14]

More recent works have considered the opportunity of using quantum-sized gold nanoclusters (NCs) presenting a sub-nanometer to ~ 2 nm core size. Unlike previously used large gold NP whose optical properties are dominated by surface plasmon resonances, gold NCs possess a molecular size and thus a non metallic electronic structure.

Over the past decade, thiolate-protected Au_{25} nanoclusters ($Au_{25}(SR)_{18}^{-}$ with R an alkyl group) have been extensively studied since they possess high thermal and chemical stabilities. [15–17] These nanoclusters present a core-shell arrangement of gold and sulphur atoms. Hence, the $Au_{25}(SR)_{18}^{-}$ system which represented in Figure 1(c) presents a C_i symmetry and is based on a central icosahedral Au_{13} core surrounded by an exterior $Au_{12}(SH)_{18}$ shell. [18] For the sake of simplicity, these $Au_{25}(SR)_{18}^{-}$ sulphur-stabilized gold nanoclusters will be referred to as gold nanoclusters (GNCs) or as Au_{25} GNCs. The quantum confinement of these GNCs yields outstanding redox, photoluminescence and catalytic properties [15,19–23]. They have already been used as catalysts [24] or as support for photoactive compounds [25,26], as they constitute promising building blocks for nano-scaled functionalised material. Thus, with the aim of elaborating photoresponsive molecule-NP hybrid devices, Au_{25} GNCs functionalised by azobenzene derivative thiolates were recently synthesised. [25] It was shown that the redox and optical absorption of the hybrid compound could be modulated after isomerisation of the azobenzene photoswitches, thus proving the interplay between the NP and the

† Electronic Supplementary Information (ESI) available: [details of any supplementary information available should be included here]. See DOI: 10.1039/b000000x/

Laboratoire Interfaces, Traitements, Organisation et Dynamique des Systèmes (ITODYS), CNRS UMR 7086, Université Paris 7 - Paris Diderot, Sorbonne Paris Cité, Bâtiment Lavoisier, 15 rue Jean Antoine de Baïf, 75205 Paris Cedex 13, France

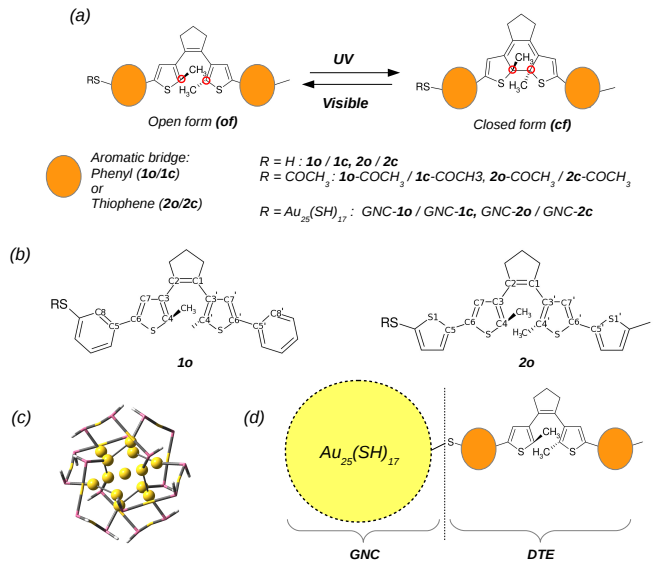

Fig. 1 (a) Dithienylethene molecules under study, **o** and **c** respectively refer to the open-ring and closed-ring isomers. (b) Atom Numbering within the **1** and **2** dithienylethene units.(c) Representation of the core (balls) -shell (tube) $Au_{25}(SH)^{-}_{18}$ GNC structure (color code: yellow=Au, pink=S, white=H). (d) Scheme of the GNC-DTE hybrid systems.

organic moiety. In the same vein, a Au_{25}-pyrene hybrid system has been synthesised.[26] In this compound, a significant fluorescence quenching was observed for the pyrene and time-resolved fluorescence upconversion and transient absorption measurements actually proved that an ultrafast electron transfer occurs from the Au_{25} to the attached pyrene. Therefore, Au_{25} GNCs can interact with an anchored organic molecule in various ways, and most of the times does not act as a simple support. This type of hybrid photoactive compounds is still very rare in the literature and the association of a GNC with photochromic molecules is potentially a unique source of novel optoelectronic properties. Consequently, there is today a great challenge to understand the electronic communication within hybrid organic-inorganic systems and the possible electron and/or energy transfer between the chromophore and the metallic GNC. In that framework, theoretical tools constitute a useful complement to experimental studies in order to design more efficient hybrid architectures.

In this theoretical study, we consider a GNC functionalized with a photochromic molecule, more precisely a DTE (see Figure 1). We do not consider an alkyl chain linker between the organic and metallic parts, as we want to maximize the communication between the DTE and the GNC. Instead, the anchoring onto the GNC is made through a covalent bond, with an aromatic bridge between the DTE unit and the binding Sulphur of the cluster. Inspired by the experimental work by Feringa and coworkers, we use two different thiol-functionalised aromatic linkers, a thiophene (molecule **1**) or a phenyl (molecule **2**) bridge, as depicted in Figure1(b). The systems under study thus correspond to $[Au_{25}(SH)_{17}$-**1**$]^{-}$ for the phenyl derivative (hereafter referred to as GNC-**1**) and $[Au_{25}(SH)_{17}$-**2**$]^{-}$ for the phenyl linker (hereafter referred to as GNC-**2**). Like in previous experimental studies dedicated to Au_{25}-pyrene hybrid systems,[26] all the systems are negatively charged (charge -1) and present a closed shell electronic structure. Both the open-ring (**o**) and closed-ring (**c**) isomers of **1** and **2** DTE molecules are considered.

As a matter of fact, theoretical chemistry can bring helpful insights to rationalize the interactions between the DTE and the GNC. We thus aim at (i) demonstrating if whether or not the photochromic properties are preserved within these new hybrid systems and (ii) investigating the possible energy and/or electron transfers between the GNC and the photoswitch. The molecular size of the GNC-DTE structures allows the use of *ab initio* quantum calculations like DFT and TD-DFT methods to explore the electronic structure and optical properties of these hybrid systems. This study is organized as follows: after a study dedicated to the optical properties of the isolated DTEs, we analyse successively the structural and optical properties of the hybrid GNC-DTE systems. Finally, we describe the possible electron and energy transfers between the molecule and the nanocluster, respectively in the framework of Förster and Rehm-Weller mechanisms.

2 Computational Details

2.1 UV-Visible absorption spectrum

To assess the optical properties of the Au_{25}-DTE hybrid systems, we rely on a three-step computational scheme, previously validated for a GNC-Pyrene system.[27]

First, to investigate the orientations that the DTE molecule can adopt with respect to the GNC, Molecular Dynamics (MD) simulations have been performed in vacuum. Experimentally, the GNC is protected with alkanethiol chains (C_6 chains).[26] Therefore, a conformational study has been carried out for the $[Au_{25}(SC_6H_{13})_{17}$-DTE$]^{-}$ system using the DL_poly code.[28] The general Amber Force Field is chosen to describe H, C, and S atoms[29] while the gold parameters are taken from the work of Ayappa et al.[30] The simulation is run following the procedure set up by Malfreyt and coworkers to study the conformation of thiolates derivatives on Gold SAMS.[31] During these simulations, we froze the positions of the Au_{25} metallic core and the sulphur atoms. These positions correspond to the X-Ray structure of $[Au_{25}(SH)_{18}]^{-}$.[18] The MD simulation procedure is described in details in the Supporting Information section. We emphasize that MD simulations only constitute a tool to generate starting structures for

the subsequent computational step.

In a second step, the following procedure has been applied: (i) Low energy conformations were randomly extracted from MD simulations. To decrease the computational cost, the seventeen (SC_6H_{13}) chains were then replaced by SH groups. Indeed, previous works have shown that these linear alkyl chains do not impact the absorption spectrum of the gold nanocluster.[18,27] (ii) For the subsequent $[Au_{25}(SH)_{17}\text{-DTE}]^-$ systems (referred to as "GNC-DTE" systems), the structure of the DTE subunit is minimized with a fixed geometry for $Au_{25}SH_{17}$. We used a DFT relativistic method relying on the zero-order regular approximation (ZORA)[32] using the Amsterdam Density Functional code (ADF).[33] At this stage, the BP86 GGA functional is chosen,[34,35] along with a triple zeta plus polarization basis set (TZP) for C, S, H, and a frozen core approximation is used for Au up to the 4*f* orbitals. Conductor-like screening model (COSMO) is used for the solvent effect description. This method was shown to yield accurate results on GNC structures.[18,27,36] (iii) All the constraints are removed and the geometry of the hybrid system is fully optimized.

Finally, we have obtained the excited-state properties using the vertical TD-DFT approximation[37,38] with the Gaussian09 software.[39] For organic conjugated compounds such as DTEs, range-separated hybrid (RSH) functionals combined with a description of solvent effects with the Polarizable Continuum Model (PCM)[40,41] allow to obtain accurate estimate of excitation energies and a description of long range phenomenon like charge transfer, a crucial problem for hybrid systems.[42,43] We have thus chosen the CAM-B3LYP[44] functional. The basis set combination, 6-31G(d) for C, S, H and LANL2DZ pseudopotential and basis set for Au, was previously found to give satisfying accuracy at a reachable computational effort.[27] A comparison of the optical properties of the $[Au_{25}(SH)_{18}]^-$ system obtained with different pseudopotentials is provided in the Supplementary Information section (see Figure S-4). Using higher quality pseudopotential / basis set does not modify the global shape of the calculated UV-Vis spectum and only yields trifling energy shifts (up to 10 nm). We have run the majority of the calculations with the PCM (Toluene) approach, since gold NP-DTE systems were previously synthesized in this solvent.[13] Within this framework, the 15 first excited states were computed for the isolated DTEs while 200 excited states were computed for each GNC-DTE hybrid system, in order to reach the electronic transitions involving the DTE moiety in the 250-300 nm region.

2.2 Emission properties

To evaluate the efficiency of the energy transfers, we have calculated the emission properties of isolated DTEs. To this purpose, we have determined the minimum on the potential energy surface corresponding to the S_1 state within the CAM-B3LYP/6-31G(d) framework. To describe the solvent effects, we have selected the state-specific (SS) approximation in its non-equilibrium limit to determine the transition energies of the excited state. The SS model accounts for the variations of the polarization of the medium following the electronic density rearrangements of the solute after emission. The emission wavelength corresponds to the longest wavelength of the vertical TD-DFT calculation computed at the minimum of the excited state.[45,46]

2.3 Free energy of electron transfer

To study photoinduced electron transfer, one has to compute the free energy of electron transfer ΔG_{ET}. A scenario leading to a positive free energy transfer is considered to be unfavourable and is then discarded. On the contrary, the more negative is the ΔG_{ET} value, the more likely is the mechanism. To compute the free energies of electron transfer, we have used a Rehm-Weller formalism:[47]

$$\Delta G_{ET} = E_{D/D^+} - E_{A/A^-} - E_{00} + w_p \quad (1)$$

where E_{D/D^+} and E_{A/A^-} represent respectively the oxidation and reduction potentials of the donor D and acceptor A, w_p is a coulombic interaction term which was demonstrated to be negligible.[48] E_{00} is a correction term due to the presence of an excited species, approximated as the vertical $S_0 \rightarrow S_1$ excitation energy. This simple formalism has been widely used to predict photoinduced electron transfer.[49–51]. Indeed, one can found other approximations to define E_{00}, such as the electronic energy difference between the relaxed ground state and the relaxed excited state, or the free energy difference between these two systems.[52] However, the two latter approximations require the optimization of the S_1 state or/and the computation of the excited state frequencies, two computational steps that are not affordable for GNC-based systems.

For the computation of the electrochemical properties, a Born-Haber cycle is used (see Supporting Information). For instance, for an oxidation process, we have:

$$\Delta G_{ox(sol)} = \Delta G_{ox(g)} + \Delta G_{solv(+I)} - \Delta G_{solv(0)} \quad (2)$$

where $\Delta G_{ox(sol)}$ and $\Delta G_{ox(g)}$ are respectively the free energy of oxidization in solution and in gas phase. $\Delta G_{solv(+I)}$ and $\Delta G_{solv(0)}$ are respectively the free energy of solvatation of the oxidized and neutral species. We have thus optimized the structure of the different systems in the gas phase, computed the harmonic vibrational frequencies in the gas phase and calculated the free energy of solvatation within the PCM model.

The oxidation potential is then given by the Nernst equation:

$$E_{D/D^+} = \frac{\Delta G_{ox(sol)}}{-nF} \quad (3)$$

with n the number of exchanged electrons and F the Faraday constant. To determine E_{A/A^-} potential, one should write the same equations based on the Born-Haber cycle and the Nernst equation for the reduction process.

Experimentally, in non-aqueous solution, the measurement is conducted with respect to a reference couple, namely Fc/Fc^+ (Ferrocene/Ferrocenium). We have thus computed absolute redox potential of the Fc/Fc^+ couple and subtract this value to the calculated absolute potential of the compound of interest.

This theoretical methodology has already been applied and validated for various organic and organometallic chemical systems[53–55] and excited redox potentials.[52,56–58] In previous theoretical works dedicated to the computation of redox potentials, it has been shown that the nature of the exchange-correlation functional plays a critical role to confront the theoretical results with experimental measurements.[59,60] Indeed, it has been demonstrated that GGA functionals provides better results than hybrid ones.[61] To compute the redox properties, we have thus chosen the BP86 functional combined with the 6-31G(d) basis set for C, S, H, and LANL2DZ pseudopotential and basis set for Au, within the PCM approach (when needed), with the Gaussian09 code. In this framework, we found that the redox potential of Fc/Fc^+ is 5.54 V in toluene and 4.99 V in dichloromethane. The reliability of this computational scheme is discussed later.

3 Optical properties of isolated DTEs

To validate the computational scheme dedicated to the optical properties, we have first studied the isolated molecules, **1** and **2**, substituted with a $-SCOCH_3$ group as synthesized by Kudernac and coworkers.[13] Deviations between the computed absorption wavelength corresponding to the first excited state and the position of the experimental absorption band are in the range of TD-DFT precision, namely 0.05 eV, 0.11 eV, and 0.02 eV for respectively **1c**-$SCOCH_3$, **2o**-$SCOCH_3$ and **2c**-$SCOCH_3$. We can thus conclude that the optical properties of the isolated DTE are accurately described within this theoretical framework.

Calculated absorption features of DTEs **1** and **2** (with R = H in Figure 1, thus corresponding to the organic fragment in the GNC-DTE compounds) obtained with this TD-DFT//DFT scheme are detailed in Table 1. For both the open-ring (**1o** and **2o**) and closed-ring (**1c** and **2c**) isomers, the less energetic transition is very intense and corresponds to a HOMO→LUMO electronic excitation. These frontier orbitals are given in Figure 2 and other relevant molecular orbitals can be found in the Supporting Information section (Figure S-1).

For **1c** and **2c**, both HOMO and LUMO are delocalised upon the entire DTE skeleton and present the typical topology of closed DTE frontier orbitals.[62] For **1o** and **2o**, the HOMO

Table 1 Most intense electronic transitions calculated at the PCM(Toluene)-CAM-B3LYP/6-31G(d)//BP86/TZP level for **1o**, **1c**, **2o** and **2c**: wavelengths (λ, in nm), oscillator strengths (f) and state description are given. Only transitions with $f \geq 0.15$ are listed in this table.

System	λ (nm)	f	Orbital composition
1o	289	0.76	HOMO→LUMO (68%)
			HOMO-1→LUMO+1 (19%)
	269	1.00	HOMO→LUMO+2 (56%)
			HOMO-1→LUMO+1 (18%)
1c	558	0.64	HOMO→LUMO (97%)
	336	0.37	HOMO-1→LUMO (72%)
			HOMO→LUMO+1 (22%)
2o	317	1.00	HOMO→LUMO (40%)
			HOMO-1→LUMO (22%)
			HOMO-1→LUMO+1 (19%)
	275	0.58	HOMO→LUMO+2 (44%)
2c	588	0.76	HOMO→LUMO (96%)
	354	0.28	HOMO→LUMO+1 (82%)

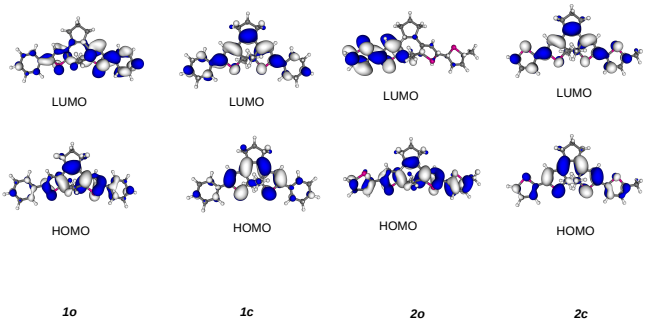

Fig. 2 Frontier molecular orbitals of **1o**, **1c**, **2o** and **2c** (threshold: 0.02 a.u).

also presents a DTE π orbital topology,[62] with an electronic density mainly centred on the photochromic core, while the LUMO is much delocalised on the lateral chains. Regarding the nature of the interaction between the two carbons involved in the cyclisation/retrocyclisation process (red-circled carbons in Figure 1), the latter orbital presents the required topology for initiating the ring closure reaction: there is a significant density on (at least one of) the reactive carbon atom(s) as well as a bonding character for the to-be-formed CC bond. The bonding interaction between the two reactive carbon atoms is highlighted in the ESI section for **1o** in Figure S-2. For **2o**, one can identify a bonding interaction between the two reactive carbon atoms by reducing the isodensity threshold (0.01 a.u instead of 0.02 a.u.) as shown in ESI (Figure S-2). The promotion of an electron towards a LUMO presenting such a topology has been shown to be the first step in the photoinduced ring-closure reaction for a large series of DTE compounds.[62–64] In the following, the promotion of an electron towards a virtual orbital presenting such a topology will be denoted as a *photochromic transition*. The presence (respectively absence) of such an electronic transition in the absorption spectrum will be used as a criterion to determine the preservation (respectively the loss) of the DTE photoreactive properties within the hybrid system.

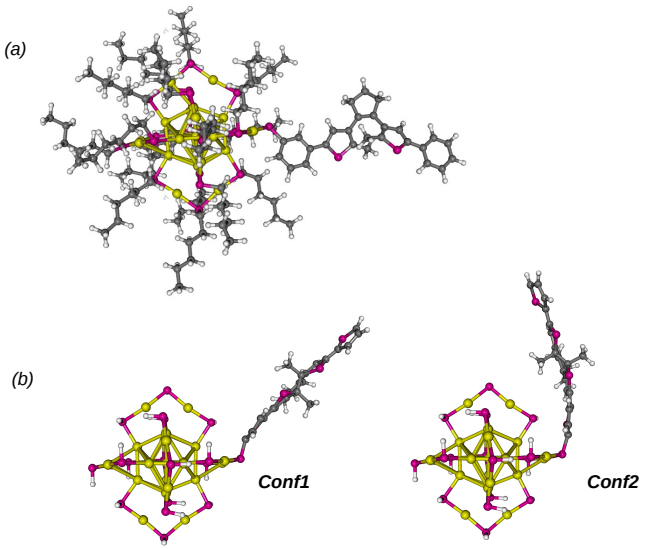

Fig. 3 (a) GNC-**1o** system coated with alkanethiol chains (color code: yellow=Au, pink=S, grey=C, white=H). (b) Example of two different conformations Conf1 and Conf2 extracted from the Molecular Dynamics simulation of GNC-**2c** (the C_6H_{13} alkane chains have been replaced by H atoms). The same color code is used.

4 GNC-DTE systems: structural, electronic and optical properties

4.1 Structural properties

Along the MD trajectory, the main parameter describing the conformation of the hybrid GNC-DTE system is the relative orientation of the photoactive molecule with respect to the nanocluster. The small size of the GNC induces a relatively large radius of curvature (see Figure 3): the 17 alkanethiol chains and the anchored DTE are thus relatively far apart and can move freely. Indeed, in the course of the MD simulation, the DTE oscillates between conformations where the DTE is tilted with respect to the GNC to more perpendicular orientations (see for instance two different conformations Conf1 and Conf2 extracted from the MD trajectory for GNC-**2c** in Figure 3). These two conformations actually correspond to the two lowest energetic conformers among a set of 20 snapshots extracted from MD simulations. The energetic difference between Conf1 and Conf2 is 4.1 kcal.mol^{-1} in favour of the Conf1 structure. In the following, we thus discuss the structural and optical properties of the Conf1 structure (referred to as GNC-**2c**).

The main geometrical parameters of the different DTEs, isolated and grafted onto the GNC, are compared in Table 2. The optimized geometries of the hybrid systems are sketched in Figure 4, for both the open and closed forms. First, one

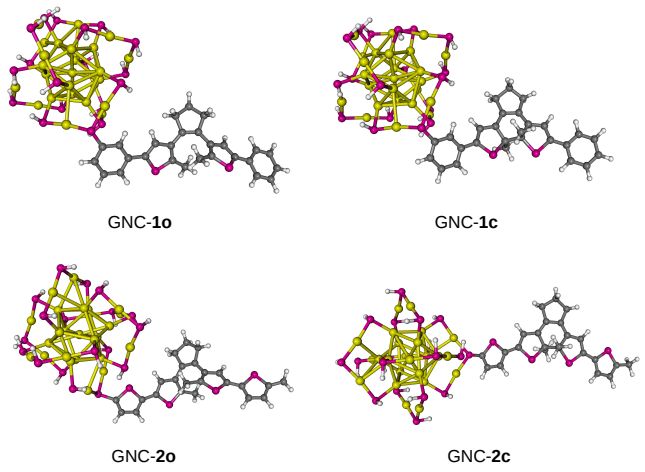

Fig. 4 Optimized geometries of the GNC-DTE systems. The GNC-**2c** structure corresponds to the Conf1 structure in Figure 3(b) with a different view angle.

Table 2 Evolution of the different structural parameters for the isolated DTE and the DTE after immobilisation on the GNC (anchored DTE). The BLA definition is provided in Supporting Information. The atom numbering is given in Figure 1. *d* is the distance between the two reactive carbon atoms C_4-$C_{4'}$. ξ_1 corresponds to the dihedral angle C_1-C_2-C_3-C_4, ξ_2 to C_2-C_1-$C_{3'}$-$C_{4'}$, ξ_3 to C_7-C_6-C_5-C_8 for **1** and C_7-C_6-C_5-S_1 for **2**, ξ_4 to $C_{7'}$-$C_{6'}$-$C_{5'}$-$C_{8'}$ for **1** and $C_{7'}$-$C_{6'}$-$C_{5'}$-$S_{1'}$ for **2**.

	1o	**1c**	**2o**	**2c**
BLA - isolated DTE (10^2)	9.041	5.152	8.695	4.471
BLA - anchored DTE (10^2)	8.672	5.431	9.244	4.488
d (Å) - isolated DTE	3.64	1.54	3.65	1.55
d (Å) - anchored DTE	3.64	1.54	3.58	1.54
$\xi_1 \setminus \xi_2$ (°) - isolated DTE	42.8\43.7	8.0\8.0	44.4\42.6	8.5\8.8
$\xi_1 \setminus \xi_2$ (°) - anchored DTE	34.2\44.2	10.2\6.6	46.9\47.6	4.9\11.5
$\xi_3 \setminus \xi_4$ (°) - isolated DTE	23.8\19.8	8.9\12.1	5.8\17.9	0.2\2.8
$\xi_3 \setminus \xi_4$ (°) - anchored DTE	2.8\19.5	32.9\11.7	1.9\20.8	8.7\5.2

can note that the anchoring on the nanocluster has a slight effect on the Bond Length Alternation (BLA) which quantifies the molecular conjugation through the difference between simple and double CC bonds along the conjugation path (see Supporting Information for a detailed description of the BLA formula). An empiric indicator of the feasibility of the ring-closure reaction is the distance *d* between the two reactive carbons. Experimentally, in crystalline samples, it has been shown that if this value exceeds 4.2 Å, the photocyclisation is expected to be compromised.[65,66] For GNC-**1o** and GNC-**2o**, *d* is respectively 3.64 and 3.65 Å, and is thus unmodified with respect to free DTEs, **1o** (3.64 Å) and **2o** (3.68 Å). In the same vein, the ξ_1 and ξ_2 dihedral angles defined in Table 2 can also impact the efficiency of the ring-closure reaction, by modifying the *d* distance. In our case, they practically do not vary after immobilization on the nanocluster, the maximum change being 8 ° between **1o** and GNC-**1o**. On the contrary, the dihedral angles ξ_3 and ξ_4, corresponding to the torsion between the first thiophene ring and the outer aromatic ring (respectively phenyl or thiophene for **1** and **2**), are significantly modified in the "anchored" conformation. For example, for **1**, ξ_3 decreases from 23.8 ° to 2.8 ° between **1o** and GNC-**1o**, and increases from 8.9 ° to 32.9 ° between **1c** and GNC-**1c**. ξ_3 is significantly more impacted than ξ_4, this torsion angle describing the moiety of the molecule close to the GNC. These geometrical perturbations will certainly echo on the optical properties of the DTE.

Concerning the relative stability between the open and closed isomers, for both isolated **1** and **2** DTEs, the energy difference between the different open/closed forms is close to 10 kcal.mol^{-1}, in favour of the open-ring isomer. This result is in accordance with previous energetic studies.[4,6] After immobilisation on the GNC, this value stays in the same order of magnitude, decreasing by circa 3 kcal.mol^{-1} for **1** and increasing by circa 2 kcal.mol^{-1} for **2**. Therefore, the presence of the metallic system does not impact the energetic difference between the open and closed isomers and does not destabilize the closed-ring form.

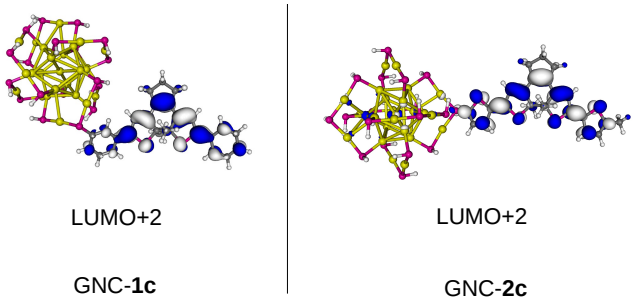

Fig. 5 Virtual molecular Orbitals of GNC-**1c** and GNC-**2c** showing a non-negligible contribution on the DTE moiety (threshold: 0.02 a.u).

4.2 Optical properties

4.2.1 Analysis methodology. As shown for the isolated DTEs, the photochromic behaviour of the molecule can be intuited from the analysis of the topology of the virtual orbitals populated after irradiation. Thus, the study of the DTE photoactive properties within the hybrid GNC-DTE compound is performed by scanning the 200 calculated excited states. We have paid a particular attention to the transitions involving DTE-localized virtual orbitals (these orbitals are shown in Figure 5) and carefully analysed their topology.

4.2.2 GNC-closed form DTE. The absorption spectra of GNC-**1c** and GNC-**2c** are presented in Figure 6. To provide a better understanding of the evolution of the DTE optical properties within the GNC-DTE system, three spectra are superimposed: the isolated DTE (in its "anchored" geometry), the GNC and the GNC-DTE. Most relevant electronic transitions are detailed in Table 3. For both systems, an intense transition

Table 3 Theoretical electronic transitions for GNC-**1o**, GNC-**2o**, GNC-**1c** and **2c** involving the DTE moiety. See Table 1 for more details.

System	λ (nm)	f	Orbital composition
GNC-**1o**	298	0.26	HOMO-3→LUMO+6 (19%)
			HOMO-2→LUMO+14 (15%)
	287	0.23	HOMO-3→LUMO+8 (45%)
			HOMO-4→LUMO+8 (39%)
	275	1.00	HOMO-3→LUMO+16 (21%)
			HOMO-3→LUMO+17 (19%)
GNC-**2o**	389	0.29	HOMO-2→LUMO+2 (23%)
			HOMO→LUMO+3 (19%)
			HOMO-1→LUMO+4 (16%)
	381	0.23	HOMO-2→LUMO+4 (28%)
			HOMO-2→LUMO+3 (20%)
			HOMO-1→LUMO+2 (18%)
			HOMO-2→LUMO+5 (10%)
	339	0.59	HOMO-3→LUMO+5 (17%)
	313	0.76	HOMO-4→LUMO+6 (20%)
GNC-**1c**	548	0.70	HOMO-1→LUMO+2 (96%)
GNC-**2c**	609	0.81	HOMO→LUMO+2 (55%)

clearly stands out in the visible region: λ = 548 nm for GNC-**1c** (oscillator strength f = 0.70) and λ = 609 nm for GNC-**2c** (f = 0.81). For these two compounds, this transition populates the LUMO+2 virtual orbital, depicted in Figure 5, which matches the LUMO of the isolated DTE. Consequently, the maximum absorption band of the closed-ring DTE is not perturbed after grafting onto the GNC.

To study the effect of the relative DTE/GNC orientation on the optical properties, another conformation (Conf2 in Figure 3(b)) was extracted from MD simulations for **2c**. Theoretical spectra corresponding to these two conformations are compared in Figure 7, with an emphasis on the visible region where the photochromic transition of the closed form is expected. No remarkable differences are observed between the spectra corresponding to these two orientations: the DTE-localised electronic transition peaks at the same wavelength, with nearly the same intensity.

From all these findings, we can thus conclude that there is no communication between the organic part and the GNC, and this yields the preservation of the optical properties of the closed-ring DTE. This lack of interaction is due to the few number of electronic transitions belonging to the metallic fragment around 600 nm. In a first order approach, the ring opening reaction is then expected to be as efficient in the hybrid system as in the free closed DTE. The preservation of the ring-opening photoreactivity heads in the same direction that the 2 nm gold NP-DTE hybrid systems. Indeed, for larger gold aggregates, Feringa *et al*[13] have shown that the absorbance spectrum of the hybrid structure is a simple addition of the NP and closed DTE optical properties, with the ring-opening of **1c** and **2c** still being efficient.

More generally, for the closed isomers, the photoactive properties are related to the position of the DTE absorption bands with respect to GNC ones. The photochromic transition is usually found around 600 nm where the absorption of the GNC is non-existent or very weak. Thus, this transition is recovered with an intensity in the same order of magnitude in the GNC-DTE spectrum. This behaviour should be preserved as long as the metallic cluster does not strongly absorb in this spectrum region.

4.2.3 GNC-open form DTE. Virtual molecular orbitals and absorption spectra of GNC-**1o** and GNC-**2o** are respectively given in Figures 8 and 9. The photochromic transitions of the open DTE are expected in the UV region, around 300 nm, where metal → metal transitions are very abundant. Therefore, the impact of the anchoring onto the GNC is not as straightforward as in the closed-isomer cases, and a thorough scan must be performed.

For GNC-**1o**, three absorption bands correspond to the promotion of an electron towards a virtual orbital localized on the DTE fragment: λ = 298 nm (f = 0.26), λ = 287 nm (f = 0.23) and λ = 275 nm (f = 1.00). As shown by Table 3, the first transition at 298 nm promotes an electron towards the LUMO+6 which possesses a non-bonding interaction between the reactive carbons. The second one populates the LUMO+8 which presents a bonding interaction between the reactive carbons and thus corresponds to a photochromic transition, according to the previously established criteria. The last transition involves the LUMO+16 and LUMO+17 which both show a bonding character between the reactive carbons. The latter transition is thus a second photochromic transition. For this compound, we thus expect the ring-closure photoactive properties to be preserved. Indeed, the experimental study of a NP-**1o** system by Feringa and co-workers led to the same results: for larger NP, the ring-closure of **1o** was found to be possible.

For GNC-**2o**, four transitions involving molecular orbitals localized on the photochrome moiety can be found: λ = 389 nm (f = 0.29), 381 nm (f = 0.23), 339 nm (f = 0.59) and 313 nm (f = 0.76). The 389 nm and 313 nm transitions populate respectively the LUMO+2 and LUMO+6, both virtual orbitals presenting a non-bonding interaction and thus a non-photochromic topology. On the opposite, the two transitions peaking respectively at 381 nm and 339 nm involve both the LUMO+2 and the LUMO+5. Since the LUMO+5 shows a bonding character between the reactive carbons (similarly to the LUMO of **2o**), these two excitations are potentially photochromic transitions. Nevertheless, the contribution of the LUMO+5 to the latter excitations is very small, 10 % for the 381 nm transition and 17 % for the 339 nm one. Moreover, contrarily to GNC-**1o**, these potentially photochromic transi-

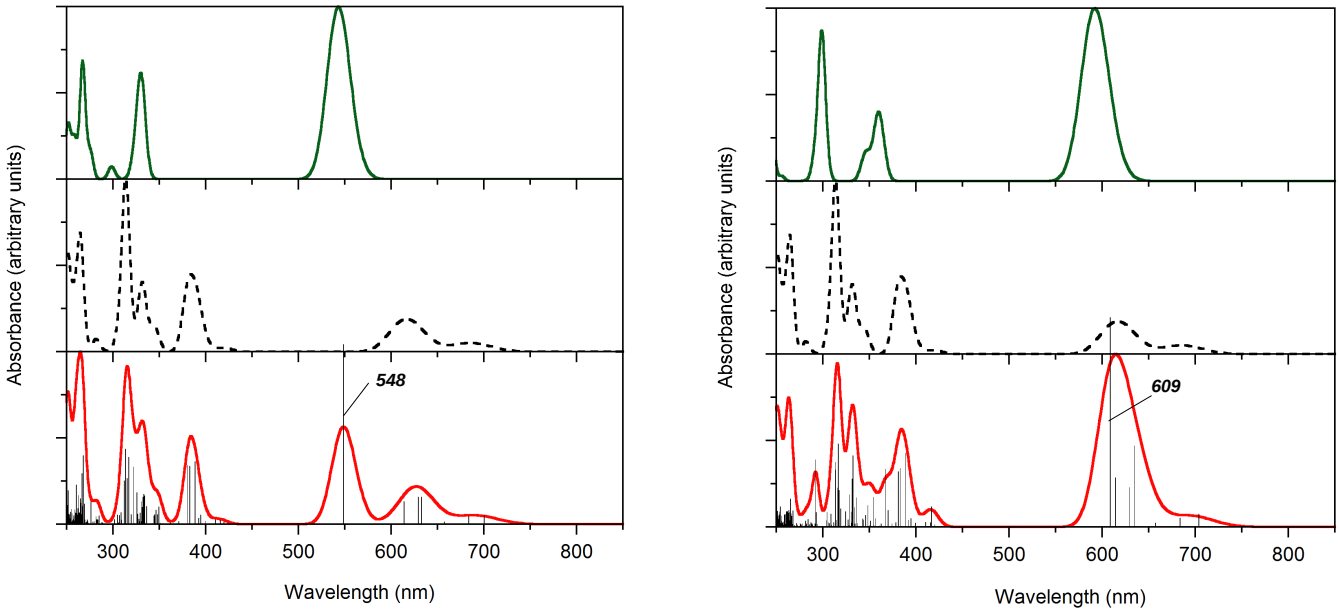

Fig. 6 Theoretical absorption spectra of GNC-**1c** (left) and GNC-**2c** (right). DTE spectrum is in green, the gold cluster spectrum is in dotted black line, and the hybrid system spectrum is in red. The calculated excitation properties are convoluted with a Gaussian function (FWHM = 0.2 eV) and the stick spectra of the hybrid systems are also represented.

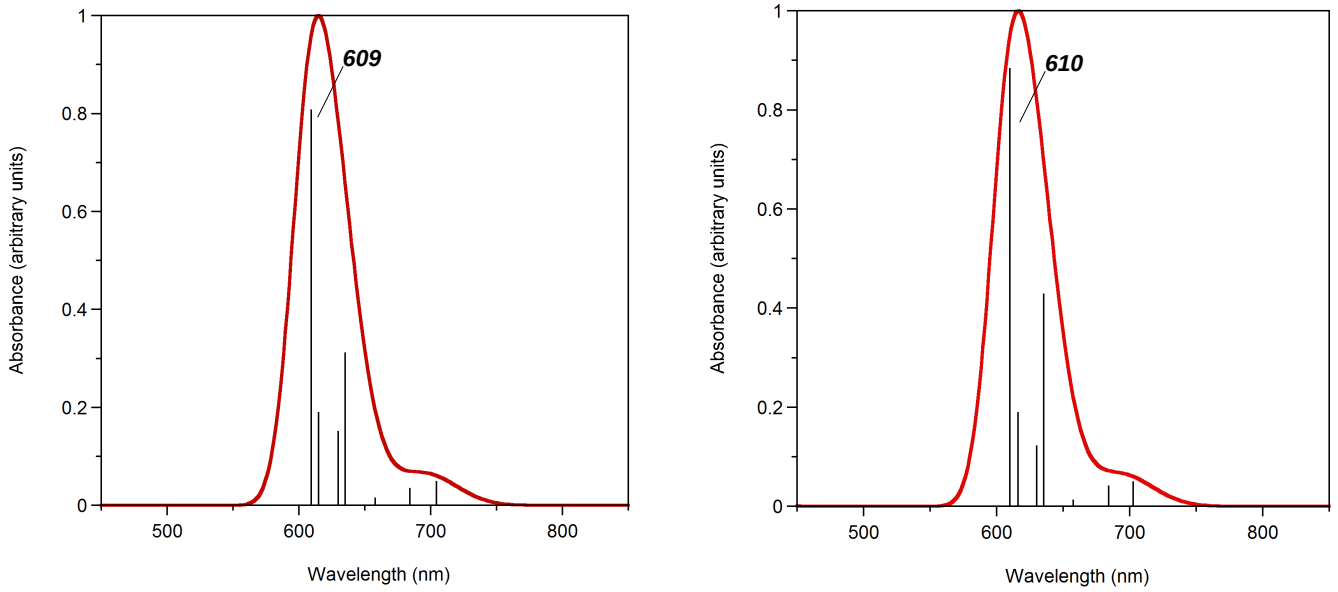

Fig. 7 Theoretical absorption spectra of GNC-**2c** for two different conformations (left: Conf1, right: Conf2) in the Visible region. These conformers are represented in Figure 3(b). The stick spectra are also represented.

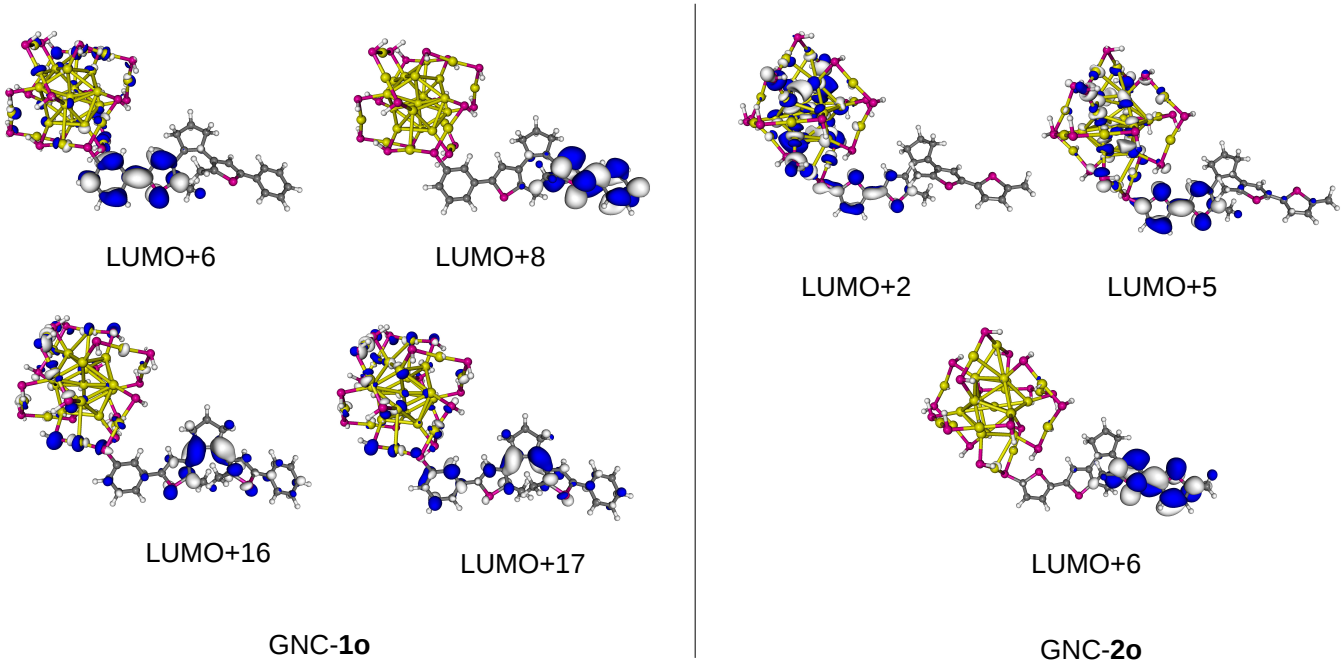

Fig. 8 Virtual molecular Orbitals of GNC-**1o** and GNC-**2o** showing a non-negligible contribution on the DTE moiety (threshold: 0.02 a.u).

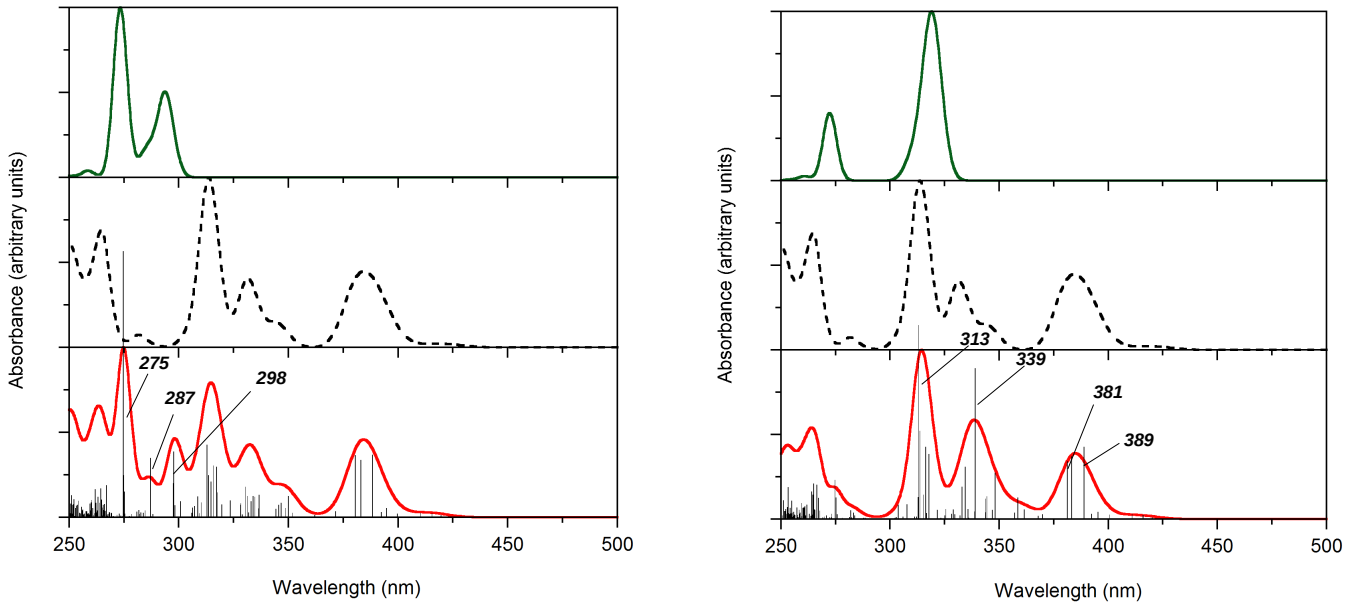

Fig. 9 Theoretical absorption spectra of GNC-**1o** (left) and GNC-**2o** (right). See Figure 6 for more details.

tions are drowned into a high density of purely metallic transitions. Consequently, among the complete absorption band including this electronic transition (in a 10 nm range), the population of the LUMO+5 becomes negligible (less than 10 %). The photochromic transition of the open DTE **2o** is then hardly recovered in the hybrid compound GNC-**2o**.

Similarly to the closed form case, we have compared the absorption features of GNC-**2o** with another stable conformation (see Figure S-6 in SI). In the UV region, there are some differences since most of the molecular orbitals of the hybrid system are delocalized on both the DTE and the GNC fragments and are thus more sensitive to the respective orientations of these two parts. Consequently, the resulting electronic excitations are slightly modified. Nevertheless, for this second conformation, one can not observe any photochromic transition presenting a non-negligible oscillator strength and the loss of the ring closure is predicted as well. For **2o** anchored on a GNC, we thus retrieve the photochromic behavior that was observed for larger gold aggregate: the ring closure should be inhibited. [13,14]

To summarise, for open hybrid systems, the preservation of the photochromic properties strongly depends on the nature of the linker between the DTE and the GNC. For the two systems under investigation GNC-**1o** and GNC-**2o**, the photochromic transition peaks in a spectrum region where the GNC absorbs as well. Thus, the optical properties of the hybrid system do not correspond to a simple addition of the DTE and metallic absorption spectra and the rationalization of the perturbation is not straightforward: only a careful analysis of the virtual orbitals can bring insights on the photoreactivity. Indeed, the mixing between metallic and DTE-localized virtual orbitals depends on the conjugated character of the DTE/GNC bridge. A closer look on the molecular orbitals in Figure 5 reveals that the virtual orbitals of GNC-**2o**, presenting a non-negligible density on the DTE moiety, still possess a consequent amount of density on the GNC. The orbital of interest for GNC-**2o**, namely the LUMO+5, is delocalised on the GNC and the bisthiophene moiety close to the metallic aggregate. In that case, due to the strong conjugated character of the bisthiophene group, the electronic structure can be described as a fragment interaction between GNC and bisthiophene, the electronic structure of the DTE core fading away. On the opposite, for GNC-**1o**, the phenyl-thiophene bridge between the DTE and the GNC is less conjugated and the DTE electronic structure is preserved. The orbital with the correct topology is then entirely localized on the DTE moiety. The preservation or loss of the photoactive properties should thus be related to the perturbation of the DTE electronic structure after immobilisation.

4.3 Electron/Energy transfer mechanism within GNC-DTE hybrid switches

Additionally to the photochromic properties, one can investigate the possible energy or electron transfer between the metallic and the organic moieties. Within this framework, we will focus on the GNC-**1** properties since we have demonstrated that only **1** should retain its switching properties once linked to the GNC.

4.3.1 Energy Transfer. Upon photoexcitation, an energy transfer following a Förster mechanism is first conceivable. [67] Such a phenomenon involving the GNC as the energy donor and a chromophore as an energy acceptor has already been observed. [68] However, for GNC-DTE systems, Au_{25} GNCs are known to emit in the 700-900 nm energy range, [69–71] and this emission band should not overlap neither the open form absorption spectrum (in the UV region) nor the closed form one (in the 500-600 nm region). Besides, it has been shown that the Au_{25} GNCs also present a blue emission with a maximum around 510 nm. [72] In that case, one can consider that the closed-ring isomer behaves as an energy acceptor, given that the fluorescence quantum yield of the GNC visible emission is not weak. Indeed, there are still some controversies about the emission properties of the GNCs and these properties cannot be rationalised with the help of TD-DFT calculations, the computational cost being prohibitive. Thus, a Förster mechanism involving the GNC as the energy donor and the closed-ring DTE as an energy acceptor cannot be ruled out. Experimental investigations of the GNCs emission properties should be carried out to confirm the existence of this mechanism.

We can also possibly consider the DTE to act as a donor and the GNC as an acceptor. The calculated emission properties of the closed DTE **1c** shows the presence of an emission band in the near IR (848 nm), a region where the GNC does not absorb. At the same time, **1o** presents a calculated emission band peaking at 345 nm, that can potentially overlaps with a GNC absorption band (see Figures 6 or 9 for the GNC absorption spectrum), as there are weak but numerous transitions lying in this area (4 transitions with f between 0.05 and 0.15, in the 330-360 nm range). Förster energy transfer is not only ruled by the amount of overlap between the donor emission band and the acceptor absorption band (see Sup. Info section for a complete description of the Förster formalism), but also by (i) the distance between the donor and the acceptor, (ii) the orientation factor κ^2 representing the orientation between the two transition dipole moments [74,75] (see Supplementary Information for the expression of κ^2) and (iii) the donor fluorescence quantum yield (QY). To enhance Förster energy transfer, (i) the spatial separation between the donor and the acceptor should be in the 10-50 Å range, which is the case in our hybrid system: GNC and the DTE are 11 Å apart. (ii) For the four GNC transition dipoles (acceptor) coupled with the

Table 4 Calculated oxidation E_{D/D^+} and reduction E_{A/A^-} potentials for DTE **1** and the GNC. Comparison with available experimental data are given in acetonitrile and dichloromethane solvents for respectively **1** and the GNC.

	E_{D/D^+} (V vs Fc/Fc$^+$)	E_{A/A^-} (V vs Fc/Fc$^+$)
1o (acetonitrile)	0.15 (exp: 1.16)	-2.85 (exp: -2.53)
1c (acetonitrile)	-0.50 (exp: 0.43)	-2.05 (exp: -1.74)
GNC (dichloromethane)	-0.55 (exp: -0.48)	-1.88 (exp:-2.36)
1o (toluene)	-0.07	-4.17
1c (toluene)	-0.75	-3.38
GNC (toluene)	-1.30	-3.32

Table 5 Free energies of electron transfer for GNC-Pyrene, GNC-**1o** and GNC-**1c** systems, for different pathways. **1o***, **1c***, GNC* and Pyrene* are the excited states of **1o**, **1c**, the GNC and the Pyrene moieties.

system	E_{00}	ΔG_{ET}
GNC $\rightarrow$ Pyrene*	433 nm ; 2.86 eV	-0.74 eV (exp: -1.37 eV[26])
Pyrene* $\rightarrow$ GNC	433 nm ; 2.86 eV	-0.42 eV (exp: -0.16 eV[26])
GNC* $\rightarrow$ Pyrene	864 nm ; 1.44 eV	0.83 eV (exp: 0.74 eV[26])
GNC $\rightarrow$ **1o***	364 nm ; 3.41 eV	-0.54 eV
1o* $\rightarrow$ GNC	364 nm ; 3.41 eV	-0.16 eV
GNC* $\rightarrow$ **1o**	864 nm ; 1.43 eV	1.44 eV
GNC $\rightarrow$ **1c***	700 nm ; 1.77 eV	0.31 eV
1c* $\rightarrow$ GNC	700 nm ; 1.77 eV	0.80 eV
GNC* $\rightarrow$ **1c**	864 nm ; 1.43 eV	0.65 eV

transition dipole of **1o** (donor) obtained by TD-DFT, κ^2 takes different values, ranging from 0 to 1.3. This calculation is led in a static framework, thus neglecting the motion leading to potential changes in the respective donor/acceptor orientation and thus consecutive modifications of the transition dipole orientations. Yet, the calculated κ^2 values are not systematically equal to zero and are in the range of the value generally used to evaluate the energy transfer efficiency (κ^2=2/3). (iii) Finally, DTE fluorescence QYs are known to be relatively weak (in the 0.01-0.1 range) since the radiative desexcitation process is in competition with the photocyclisation reaction.[76] Therefore, from the last observation, we can intuit that the emission properties of the DTE should weaken the efficiency of the energy transfer and may even prohibit this mechanism, with the DTE acting as a donor and the GNC as an acceptor.

4.3.2 Electron Transfer. Au_{25} GNCs are well known to switch between different charge states, especially from the natural negatively charged form to the neutral form.[77] Furthermore, electron transfer involving the GNC and an organic chromophore has already been observed.[26,78] In particular, Devadas and co-workers have actually proved that an ultrafast electron transfer occurs from the Au_{25} NC to an attached excited pyrene derivative.[26]

In that framework, we have first validated the protocol aiming at calculating the free energies of electron transfer. Concerning the redox properties, Table 4 shows that the calculated potentials are globally in good agreement with reported experimental values (for instance, the calculated and experimental oxidation potential of the GNC are respectively -0.48 and -0.55 V), except for the oxidation potential of the closed form DTE.

Concerning the Rehm-Weller formalism, in a first step, we have considered the GNC/Pyrene system and compared the free energies of electron transfer experimentally obtained by Devadas *et al*[26] to theoretical values calculated with our methodology. We have determined the structural, electronic and optical properties of the GNC-Pyrene system in a previous work.[27] Table 5 shows that the evolution of ΔG_{ET} value obtained by Devadas and coworkers is reproduced with our calculation scheme: the electron transfer from the excited Pyrene to the GNC is the unique favourable mechanism, indicating that this transfer is uni-directional.

In the same vein, to investigate the electron transfer mechanism within the GNC-DTE hybrid system, three possible pathways might be investigated: i) from the GNC to the excited DTE (open or closed), ii) from the excited DTE (open or closed) to the GNC, iii) from the excited GNC to the DTE (open or closed). For GNC-DTE systems, the comparison of the three pathways leads to the following results: an electron transfer may only occur between the DTE open form and the GNC. For pathways involving the closed form **1c**, the calculated free energy values are always positive and thus unfavourable to the existence of any electron transfer between the two moieties. Additionally, the possible electron transfer between **1o** and the GNC is found to be uni-directional: the most favorable ΔG_{ET} value is obtained for the GNC $\rightarrow$ **1o*** mechanism. One can note that this electron transfer from the GNC to the excited open DTE should not quench the photocyclization reaction: the S_1 of **1o** (which is the photochromic transition) will still be populated (the electron transfer from **1o** to the GNC is less favorable), as needed for the ring closure. It should thus be possible to control the electron transfer by light induced switching: for the open-ring isomer, there is an electron transfer from the GNC to the excited DTE while, after photoirradiation and formation of the closed-ring isomer, the electron transfer between the organic and metallic moieties is impeded.

5 Conclusions

This work enlightens the possible functionalities of new hybrid compounds, built upon a Au_{25} nanocluster functionalized with a DTE photochromic unit. By combining DFT and TD-DFT calculation schemes, we have first investigated the

photochromic properties of these new hybrid systems. While the DTE ring-opening reaction should not be impacted by the grafting onto the GNC, the ring-closure reaction might be impeded. The preservation or loss of the photoactive properties actually depends on the nature of the aromatic linker bridging the dithienylethene moiety and the gold cluster. In some cases (in particular with a thiophene linker), the impossibility to photo-close the open-ring isomer can be explained by the impossibility to populate a virtual orbital possessing a bonding interaction between the two carbons atoms involved in the bond formation. Hence, we demonstrate that the perturbation of the DTE electronic structures due to the grafting onto the GNC can rationalize the modification of the photoswitching properties, without referring to any dynamical effect observed upon photoexcitation: the loss of photoactive properties should not be systematically caused by a quenching of the excited states.

In a second step, for the GNC-**1o** and GNC-**1c** systems, where the photoreactivity is still efficient, we have investigated the possible energy and electron transfer mechanisms between the GNC and the DTE moieties. On the one hand, due to the weak emission properties of the DTE open-ring isomer, energy transfer following a Förster mechanism from the excited open photochrom to the metallic cluster can be ruled out. The energy transfer from the excited GNC to the closed-ring DTE may be conceivable, given that the fluorescence quantum yield of the GNC visible emission is not weak. On the other hand, by using a Rehm-Weller formalism, we demonstrate that a uni-directional electron transfer may occur, from the GNC to the excited open-form DTE. Switching from the DTE open-ring isomer to the close one should thus enable to light-control the electron transfer within this hybrid system. Hence, this study sheds light upon a potential new family of hybrid system, with bi-functional switching capacities, combining the photochomism to a uni-directional electron transfer, and paves the way towards promising future experimental works.

6 Acknowledgement

This research used resources of the GENCI-CINES/IDRIS (Grant c2011086680) and the ITODYS local cluster.

7 Supporting Information

The following additional informations are available: the Molecular Dynamics procedure ; Molecular orbitals involved in electronic transitions of the isolated DTEs ; Bond Length Alternation calculation ; Absorption spectra of the GNC: comparison of different pseudoptentials ; Absorption spectra of GNC-**1o** and GNC-**2o** ; Effect of the conformation on the optical properties of GNC-**2o** in the 250-850 nm range ; Förster energy transfer formalism ; Born-Haber thermodynamic cycle used for the computation of the electrochemical properties ; IR spectra of GNC-**1o** and GNC-**1c**.

References

1 M. Irie, T. Lifka, S. Kobatake and N. Kato, *J. Am. Chem. Soc.*, 2000, **122**, 4871–4876.
2 S. Kobatake, T. Yamada, K. Uchida, N. Kato and M. Irie, *J. Am. Chem. Soc.*, 1999, **121**, 2380–2386.
3 K. Matsuda and M. Irie, *J. Photochem. Photobiol., C*, 2004, **5**, 169 – 182.
4 M. Irie, *Chem. Rev.*, 2000, **100**, 1685–1716.
5 F. Meng, Y.-M. Hervault, L. Norel, K. Costuas, C. Van Dyck, V. Geskin, J. Cornil, H. H. Hng, S. Rigaut and X. Chen, *Chem. Sci.*, 2012, **3**, 3113–3118.
6 P. D. Patel and A. E. Masunov, *J. Phys. Chem. C*, 2011, **115**, 10292–10297.
7 P. Patel and A. Masunov, *Computational Science ICCS 2009*, Springer Berlin Heidelberg, 2009, vol. 5545, pp. 211–220.
8 S. Nakamura, S. Yokojima, K. Uchida, T. Tsujioka, A. Goldberg, A. Murakami, K. Shinoda, M. Mikami, T. Kobayashi, S. Kobatake, K. Matsuda and M. Irie, *J. Photochem. Photobiol., A*, 2008, **200**, 10 – 18.
9 A. Perrier, F. Maurel and D. Jacquemin, *Acc. Chem. Res.*, 2012, **45**, 1173–1182.
10 H. Nishi, T. Asahi and S. Kobatake, *Phys. Chem. Chem. Phys.*, 2012, **14**, 4898–4905.
11 H. Nishi, T. Asahi and S. Kobatake, *J. Phys. Chem. C*, 2009, **113**, 17359–17366.
12 H. Nishi, T. Asahi and S. Kobatake, *J. Phys. Chem. C*, 2011, **115**, 4564–4570.
13 T. Kudernac, S. van der Molen, B. J. van Wees and B. Feringa, *Chem. Commun.*, 2006, **34**, 3597–3599.
14 D. Dulić, S. J. van der Molen, T. Kudernac, H. T. Jonkman, J. J. D. de Jong, T. N. Bowden, J. van Esch, B. L. Feringa and B. J. van Wees, *Phys. Rev. Lett.*, 2003, **91**, 207402.
15 H. Qian, M. Zhu, Z. Wu and R. Jin, *Acc. Chem. Res.*, 2012, **45**, 1470–1479.
16 T. G. Schaaff, G. Knight, M. N. Shafigullin, R. F. Borkman and R. L. Whetten, *J. Phys. Chem. B*, 1998, **102**, 10643–10646.
17 R. L. Donkers, D. Lee and R. W. Murray, *Langmuir*, 2004, **20**, 1945–1952.
18 M. Zhu, C. M. Aikens, F. J. Hollander, G. C. Schatz and R. Jin, *J. Am. Chem. Soc.*, 2008, **130**, 5883–5885.
19 M. Walter, J. Akola, O. Lopez-Acevedo, P. D. Jadzinsky, G. Calero, C. J. Ackerson, R. L. Whetten, H. Grnbeck and H. Hkkinen, *Proc. Natl. Acad. Sci. U. S. A.*, 2008, **105**, 9157–9162.
20 R. B. Wyrwas, M. M. Alvarez, J. T. Khoury, R. C. Price, T. G. Schaaff and R. L. Whetten, *Eur. Phys. J. D*, 2007, **43**, 91–95.
21 O. Varnavski, G. Ramakrishna, J. Kim, D. Lee and T. Goodson, *J. Am. Chem. Soc.*, 2010, **132**, 16–17.
22 J. F. Parker, C. A. Fields-Zinna and R. W. Murray, *Acc. Chem. Res.*, 2010, **43**, 1289–1296.
23 Y. Negishi, K. Nobusada and T. Tsukuda, *J. Am. Chem. Soc.*, 2005, **127**, 5261–5270.
24 Y. Zhu, H. Qian and R. Jin, *Chem. - Eur. J.*, 2010, **16**, 11455–11462.
25 Y. Negishi, U. Kamimura, M. Ide and M. Hirayama, *Nanoscale*, 2012, **4**, 4263–4268.
26 M. S. Devadas, K. Kwak, J.-W. Park, J.-H. Choi, C.-H. Jun, E. Sinn, G. Ramakrishna and D. Lee, *J. Phys. Chem. Lett.*, 2010, **1**, 1497–1503.

27 A. Fihey, F. Maurel and A. Perrier, *J. Phys. Chem. C*, 2014, **118**, 4444–4453.
28 W. Smith, C. Yong and P. Rodger, *Mol. Simul.*, 2002, **28**, 385–471.
29 W. D. Cornell, P. Cieplak, C. I. Bayly, I. R. Gould, K. M. Merz, D. M. Ferguson, D. C. Spellmeyer, T. Fox, J. W. Caldwell and P. A. Kollman, *J. Am. Chem. Soc.*, 1995, **117**, 5179–5197.
30 B. Rai, S. P., C. P. Malhotra, Pradip and K. G. Ayappa, *Langmuir*, 2004, **20**, 3138–3144.
31 G. Filippini, Y. Israeli, F. Goujon, B. Limoges, C. Bonal and P. Malfreyt, *J. Phys. Chem. B*, 2011, **115**, 11678–11687.
32 E. van Lenthe, A. Ehlers and E.-J. Baerends, *J. Chem. Phys.*, 1999, **110**, 8943–8953.
33 G. te Velde, F. M. Bickelhaupt, E. J. Baerends, C. Fonseca Guerra, S. J. A. van Gisbergen, J. G. Snijders and T. Ziegler, *J. Comput. Chem.*, 2001, **22**, 931–967.
34 A. D. Becke, *Phys. Rev. A*, 1988, **38**, 3098–3100.
35 J. P. Perdew and Y. Wang, *Phys. Rev. B*, 1992, **45**, 13244–13249.
36 C. M. Aikens, *J. Phys. Chem. A*, 2009, **113**, 10811–10817.
37 E. Runge and E. K. U. Gross, *Phys. Rev. Lett.*, 1984, **52**, 997–1000.
38 R. Bauernschmitt and R. Ahlrichs, *Chem. Phys. Lett.*, 1996, **256**, 454 – 464.
39 M. J. Frisch, G. W. Trucks, H. B. Schlegel, G. E. Scuseria, M. A. Robb, J. R. Cheeseman, G. Scalmani, V. Barone, B. Mennucci, G. A. Petersson, H. Nakatsuji, M. Caricato, X. Li, H. P. Hratchian, A. F. Izmaylov, J. Bloino, G. Zheng, J. L. Sonnenberg, M. Hada, M. Ehara, K. Toyota, R. Fukuda, J. Hasegawa, M. Ishida, T. Nakajima, Y. Honda, O. Kitao, H. Nakai, T. Vreven, J. A. Montgomery, Jr., J. E. Peralta, F. Ogliaro, M. Bearpark, J. J. Heyd, E. Brothers, K. N. Kudin, V. N. Staroverov, R. Kobayashi, J. Normand, K. Raghavachari, A. Rendell, J. C. Burant, S. S. Iyengar, J. Tomasi, M. Cossi, N. Rega, J. M. Millam, M. Klene, J. E. Knox, J. B. Cross, V. Bakken, C. Adamo, J. Jaramillo, R. Gomperts, R. E. Stratmann, O. Yazyev, A. J. Austin, R. Cammi, C. Pomelli, J. W. Ochterski, R. L. Martin, K. Morokuma, V. G. Zakrzewski, G. A. Voth, P. Salvador, J. J. Dannenberg, S. Dapprich, A. D. Daniels, O. Farkas, J. B. Foresman, J. V. Ortiz, J. Cioslowski and D. J. Fox, *Gaussian 09 Revision A.1*, Gaussian Inc. Wallingford CT 2009.
40 J. Tomasi, B. Mennucci and R. Cammi, *Chem. Rev.*, 2005, **105**, 2999–3094.
41 M. Cossi and V. Barone, *J. Chem. Phys.*, 2001, **115**, 4708–4717.
42 D. Jacquemin, E. A. Perpète, I. Ciofini and C. Adamo, *Acc. Chem. Res.*, 2009, **42**, 326–334.
43 D. Jacquemin, B. Mennucci and C. Adamo, *Phys. Chem. Chem. Phys.*, 2011, **13**, 16987.
44 T. Yanai, D. P. Tew and N. C. Handy, *Chem. Phys. Lett.*, 2004, **393**, 51 – 57.
45 B. Mennucci, *J. Phys. Chem. Lett.*, 2010, **1**, 1666–1674.
46 D. Jacquemin, A. Planchat, C. Adamo and B. Mennucci, *J. Chem. Theory Comput.*, 2012, **8**, 2359–2372.
47 D. Rehm and A. Weller, *Isr. J. Chem.*, 1970, **8**, 259–271.
48 J. L. Goodman and K. S. Peters, *J. Am. Chem. Soc.*, 1986, **108**, 1700–1701.
49 X. Zhang, L. Chi, S. Ji, Y. Wu, P. Song, K. Han, H. Guo, T. D. James and J. Zhao, *J. Am. Chem. Soc.*, 2009, **131**, 17452–17463.
50 C. J. Fahrni, L. Yang and D. G. VanDerveer, *J. Am. Chem. Soc.*, 2003, **125**, 3799–3812.
51 P. Kubat, J. Sebera, S. Zalis, J. Langmaier, M. Fuciman, T. Polivka and K. Lang, *Phys. Chem. Chem. Phys.*, 2011, **13**, 6947–6954.
52 B. Camino, M. D. L. Pierre and A. M. Ferrari, *J. Mol. Struct.*, 2013, **1046**, 116 – 123.
53 S. J. Konezny, M. D. Doherty, O. R. Luca, R. H. Crabtree, G. L. Soloveichik and V. S. Batista, *J. Phys. Chem. C*, 2012, **116**, 6349–6356.
54 M. Namazian, C. Y. Lin and M. L. Coote, *J. Chem. Theory Comput.*, 2010, **6**, 2721–2725.
55 L. Castro and M. Bhl, *J. Chem. Theory Comput.*, 2014, **10**, 243–251.
56 C. Qin and A. E. Clark, *Chem. Phys. Lett.*, 2007, **438**, 26 – 30.
57 M. Pastore, S. Fantacci and F. De Angelis, *J. Phys. Chem. C*, 2010, **114**, 22742–22750.
58 C. Climent and D. Casanova, *Chem. Phys.*, 2013, **423**, 157 – 166.
59 L. E. Roy, E. Jakubikova, M. G. Guthrie and E. R. Batista, *J. Phys. Chem. A*, 2009, **113**, 6745–6750.
60 J. J. Guerard and J. S. Arey, *J. Chem. Theory Comput.*, 2013, **9**, 5046–5058.
61 L. E. Roy, E. Jakubikova, M. G. Guthrie and E. R. Batista, *The Journal of Physical Chemistry A*, 2009, **113**, 6745–6750.
62 A. Fihey, A. Perrier and F. Maurel, *J. Photochem. Photobiol., A*, 2012, **247**, 30–41.
63 A. D. Laurent, J.-M. André, E. A. Perpète and D. Jacquemin, *J. Photochem. Photobiol., A*, 2007, **192**, 211 – 219.
64 A. Perrier, S. Tesson, D. Jacquemin and F. Maurel, *Comp. Theor. Chem.*, 2012, **990**, 167–176.
65 A. Perrier, F. Maurel and D. Jacquemin, *J. Phys. Chem. C*, 2011, **115**, 9193–9203.
66 S. Kobatake, M. Morimoto, Y. Asano, A. Murakami, S. Nakamura and M. Irie, *Chem. Lett.*, 2002, **31**, 1224–1225.
67 B. Valeur and M. N. Berberan-Santos, in *Excitation Energy Transfer*, Wiley-VCH Verlag GmbH and Co. KGaA, 2012, pp. 213–261.
68 M. A. H. Muhammed, A. K. Shaw, S. K. Pal and T. Pradeep, *J. Phys. Chem. C*, 2008, **112**, 14324–14330.
69 M. S. Devadas, J. Kim, E. Sinn, D. Lee, T. Goodson and G. Ramakrishna, *J. Phys. Chem. C*, 2010, **114**, 22417–22423.
70 Z. Wu and R. Jin, *Nano Lett.*, 2010, **10**, 2568–2573.
71 M. S. Devadas, V. D. Thanthirige, S. Bairu, E. Sinn and G. Ramakrishna, *J. Phys. Chem. C*, 2013, **117**, 23155–23161.
72 G. Ramakrishna, O. Varnavski, J. Kim, D. Lee and T. Goodson, *J. Am. Chem. Soc.*, 2008, **130**, 5032–5033.
73 S. H. Yau, O. Varnavski, J. D. Gilbertson, B. Chandler, G. Ramakrishna and T. Goodson, *J. Phys. Chem. C*, 2010, **114**, 15979–15985.
74 J. Martensson, *Chem. Phys. Lett.*, 1994, **229**, 449 – 456.
75 M. Pastore and F. D. Angelis, *J. Phys. Chem. Lett.*, 2012, **3**, 2146–2153.
76 S. Aloise, M. Sliwa, G. Buntinx, S. Delbaere, A. Perrier, F. Maurel, D. Jacquemin and M. Takeshita, *Phys. Chem. Chem. Phys.*, 2013, **15**, 6226–6234.
77 S. Antonello, G. Arrigoni, T. Dainese, M. De Nardi, G. Parisio, L. Perotti, A. Ren, A. Venzo and F. Maran, *ACS Nano*, 2014, **8**, 2788–2795.
78 Z. Liu, Q. Xu, S. Jin, S. Wang, G. Xu and M. Zhu, *Int. J. Hydrogen Energy*, 2013, **38**, 16722 – 16726.